ANALYSIS OF CONJUGATE HEAT TRASFER PROBLEM IN A MICROCHANNEL FOR A MIXED ELECTRO-OSMOTIC/PRESSURE DRIVEN FLOW OF A FLUID WITH A REOLOGICAL POWER LAW MODEL

Juan P. Escandón[a], Oscar E. Bautista[a], Federico Mendéz[b] and Eric Bautista[a]

[a]*Departamento de Termofluidos, SEPI-ESIME Azcapotzalco, México D. F., 02250, México, jescandon@ipn.mx, http://www.sepi.esimeazc.ipn.mx/*

[b]*Departamento de Termofluidos, Facultad de Ingeniería UNAM, México D. F., 02250, México, http://www.ingenieria.unam.mx/*

Keywords: power law model, conjugated heat transfer, electro-osmotic, microchannel.

Abstract. In this work we solve numerically the conjugated heat transfer problem in steady state of a non-Newtonian fluid and solid walls in a microchannel under the influence of pressure and electro-osmotic forces. The velocity field is determined taking into account a hydrodynamically fully-developed flow and a constitutive relation based in a rheological power law model. The numerical process results in: velocity profiles of the flow and in the solid-fluid temperature distributions. It is shown the influence of nondimensional parameters involved in the analysis on the conjugated heat transfer problem: the Peclet number, a normalized power generation term being the ratio of heat flow from the external wall to the Joule heating, a conjugation term which determines the basic heat transfer regimes between fluid and solid sections in the microchannel. For the flow field: an indicator of non Newtonian behavior, an electrokinetic parameter and a ratio of pressure forces to the electro-osmotic forces, the last acts on the flow as a drag reducer and drag increaser under favorable and adverse pressure gradients, respectively. An asymptotic solution was introduced to validate the numerical process.

1   INTRODUCTION

The microfluidic devices are used in the handling of biomedical and chemical analysis. Thus, electrokinetic transport is widely used to control flow and for manipulate sample solutes, include injection, separation, mixing, dilution/concentration, and reaction. Originally, the electrokinetic transport operates a combination of two mechanisms drivers: electrophoresis and electro-osmosis. Electrophoresis is the migration of charged solutes in an electrolyte under an applied electric field; the electro-osmosis gives the movement of a volume of an aqueous solution adjacent to a solid charged surface when an external electric field is applied tangentially along the surface (Tang et al., 2007). Due to the rapid development of "Lab-on-a-Chip" technologies during recent years, electro-osmosis is being used extensively as a driving force for manipulating fluid flows for transport and control samples in nano volumes of fluids to biological, chemical and medical diagnostics. Advances in microfluidic devices make possible a complete analysis of fluids in the biochemistry area in a single fabricated chip; therefore, it is fundamental understand the characteristics of fluids flow in microchannels to have an optimum design and precise control of microfluidics devices (Zhao et al., 2008).

The physics of electrokinetic phenomena and specifically in the electro-osmotic and electrophoretic flow has been extensively reviewed in the literature (Masliyah, 2006; Karniadaski, 2005; Li, 2004). The heat transfer phenomena in microchannels has been studied by Xuan (2004a, b), and Tang (2004a, b; 2007), they analyze the coupled cases with temperature and conjugates problems in electro-osmotic flow, and is emphasized the inevitable effect of Joule heating in the flow. Such works in this paragraph are under consideration of Newtonian fluids, its only considers the part of the solvent in the flow, and some are in transient state.

So, with the advent of electrokinetics for the transport of chemical and biological fluids through biochips, it is necessary to mathematically characterize the transport mechanisms associated with the process for efficient design of microfluidic systems. Strategies for characterization are based on electro-osmotic transport of Newtonian fluids, however, that consideration may be somewhat inappropriate for some applications. It´s clear that a model such as Newton's law of viscosity may be insufficient to fully describe the constitutive behavior of chemical and biological complex fluids. Although in the literature there are several models proposed to analyze the behavior of non Newtonian fluids, at present, still appear relevant implications on the transport of electrokinetic flows that have not been completely resolved by the scientific community (Das and Chakraborty, 2006). Studies by Zhao et al. (2008), Berli (2008) and Tang et al. (2009), in this regard consider the power law for non Newtonian fluids and only solve the hydrodynamics of electro-osmotic flow; Das and Chakraborty (2006) also uses the power law to solve analytically the distribution of velocity, temperature and concentration on electro-osmotic flows of non Newtonian biological fluids, but without consider the conjugate heat transfer problem in the microchannel wall; Park (2008) presents a numerical hydrodynamics investigation for electro-osmotic flow of non Newtonian fluids as blood and DNA through microchannels, where is adapted the concept of the Helmholtz-Smoluchowski velocity for viscoelastic fluids. An analytical solution for the fluid flow has been presented by Afonso (2009) for non Newtonian fluids in steady state and fully developed flow in microchannels of parallel plates and pipes, this work shows the combined effects of the rheology of the fluid and the gradients of electro-osmotic and pressure

forces on the velocity distribution; the viscoelastic fluids employees describe the constitutive Phan-Thien Thaner model, and is an approximation of studies of fluids such as blood, saliva, synovial and other biofluids.

2 METHODOLOGY

2.1 Physical model

The Figure 1 shows a squematic view of the physical model, the fluid flow is through of a microchannel formed by two parallel flat plates of height $2H$, length L, and width w, the wall thickness is H_w. $L/H \gg 1$, $L/H_w \gg 1$, $w/H \gg 1$, $w/H_w \gg 1$. We considered a fluid with a rheological power law model. The driving forces are provided by an electric field E_x and a pressure gradient p_x in the axial direction between inlet and outlet of microchannel. For analysis, properties are considered constant with the temperature; the heat transfer its in steady state and flow hydrodynamically developed. The fluid enters at a temperature T_e in $x = 0$. The wall has adiabatic conditions in $x < 0$ and $x > L$. To $0 \leq x \leq L$ there is a constant heat flux q_0'' in the external wall.
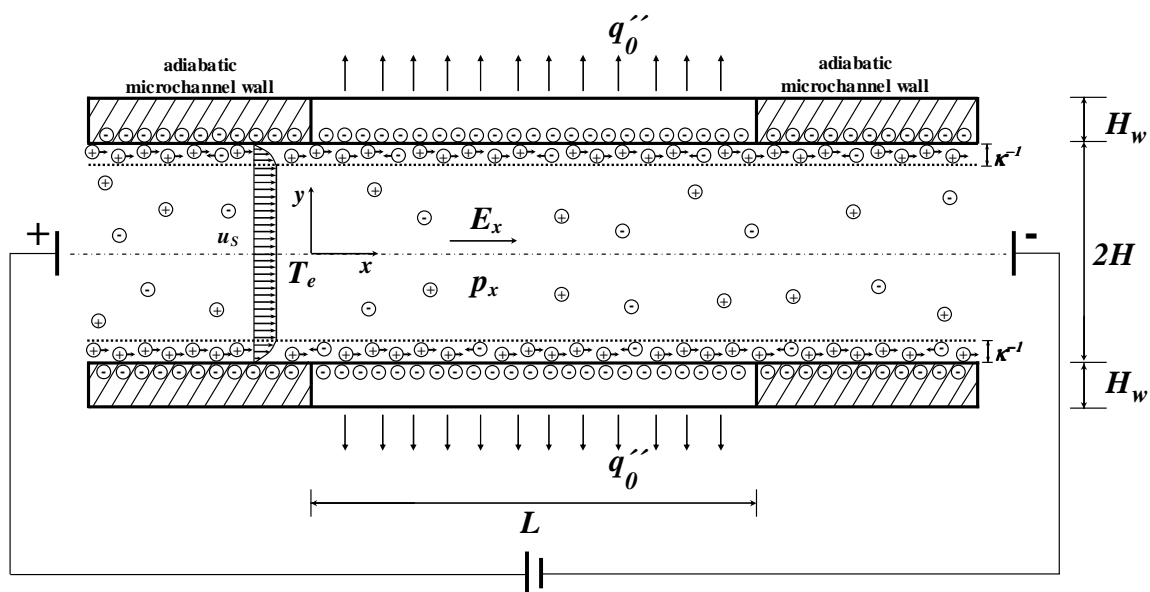
Figure 1. Schematic of mixed electro-osmotic and pressure driven flow between two parallel flat plates.

2.2 Energy equations

The energy equation for the fluid is given by

$$\rho C_{pf} u \frac{\partial T}{\partial x} = k_f \frac{\partial^2 T}{\partial x^2} + k_f \frac{\partial^2 T}{\partial y^2} + \sigma E_x^2, \tag{1}$$

where ρ, C_{pf}, T, k_f, σ and u are the density, the specific heat, the temperature, the thermal conductivity, the electrical conductivity and the axial velocity component of the fluid respectively; x, y are the axial and the transversal coordinate. The boundary conditions

associated with Eq. (1) are

$$x = 0 : T = T_e, \tag{2a}$$

$$x = L : \frac{\partial T}{\partial x} = 0, \tag{2b}$$

$$y = 0 : \frac{\partial T}{\partial y} = 0, \tag{2c}$$

$$y = H : T_w = T ; -k_w \frac{\partial T_w}{\partial y} = -k_f \frac{\partial T}{\partial y}, \tag{2d}$$

where T_w, and k_w are the temperature and the thermal conductivity in the wall, respectively.

The energy equation for the solid is given by

$$\frac{\partial^2 T_w}{\partial x^2} + \frac{\partial^2 T_w}{\partial y^2} = 0, \tag{3}$$

with their boundary conditions associated

$$x = 0 : \frac{\partial T_w}{\partial x} = 0, \tag{4a}$$

$$x = L : \frac{\partial T_w}{\partial x} = 0, \tag{4b}$$

$$-k_w \frac{\partial T_w}{\partial y} \bigg|_{y = H + H_w} = q_0'', \tag{4c}$$

$$y = H : T_w = T ; -k_w \frac{\partial T_w}{\partial y} = -k_f \frac{\partial T}{\partial y}. \tag{4d}$$

Defining the following dimensionless variables

$$\chi = \frac{x}{L}, \tag{5a}$$

$$\eta = \frac{y}{H}, \tag{5b}$$

$$\bar{u} = \frac{u}{u_S}, \tag{5c}$$

$$\theta = \frac{k_f (T - T_e)}{\sigma E_x^2 H^2}, \tag{5d}$$

$$\theta_w = \frac{k_f (T_w - T_e)}{\sigma E_x^2 H^2}, \tag{5e}$$

$$Z = \frac{y - H}{H_w}, \tag{5f}$$

where χ and η are the dimensionless axial and the transversal coordinates respectively; $\bar{u}$, θ, θ_w and Z are the velocity, the temperature in the fluid, the temperature in the solid and the transversal coordinate to analyze the solid wall, dimensionless, respectively. $u_S = -n\kappa^{\frac{1-n}{n}}(\in \zeta E_x/m)^{\frac{1}{n}}$ is the generalized Soluchowski velocity for power law fluids (Zhao et al, 2008); $\in$, ζ, n, m and κ are the dielectric constant of the fluid, the Zeta potential in the shear plane of the double electric layer (EDL), the flow consistency index, the flow behavior index and the inverse Debye length, respectively. By introduce the appropriate dimensionless variables from Eq. (5) in Eq. (1-2) is obtained the dimensionless energy equation to the fluid region into microchannel

$$\beta Pe\bar{u}\frac{\partial \theta}{\partial \chi} = \beta^2 \frac{\partial^2 \theta}{\partial \chi^2} + \frac{\partial^2 \theta}{\partial \eta^2} + 1, \tag{6}$$

and their boundary conditions

$$\chi = 0 : \theta = 0 \tag{7a}$$

$$\chi = 1 : \frac{\partial \theta}{\partial \chi} = 0 \tag{7b}$$

$$\eta = 0 : \frac{\partial \theta}{\partial \eta} = 0 \tag{7c}$$

$$\eta = 1 : \theta = \theta_w \tag{7d}$$

in addition to Eq. (7d) was considered the next boundary condition in the internal interface of microchannel from the Eq. (2d)

$$\frac{\bar{\alpha}}{\bar{\varepsilon}^2}\frac{\partial \theta_w}{\partial Z}\bigg|_{Z=0} = \frac{\partial \theta}{\partial \eta}\bigg|_{\eta=1} \tag{8}$$

Then, the energy equation in the fluid and their boundary conditions leaves the following dimensionless parameters

$$\beta = \frac{H}{L}, \tag{9a}$$

$$\bar{\varepsilon} = \frac{H_w}{L}, \tag{9b}$$

$$Pe = \frac{\rho C_{pf} u_S H}{k_f}, \tag{9c}$$

$$\bar{\alpha} = \frac{k_w}{k_f}\frac{H}{L}\frac{H_w}{L}, \tag{9d}$$

where β and $\bar{\varepsilon}$ are the aspect ratios in the fluid and solid region, respectively; Pe and $\bar{\alpha}$ are the Peclet number and the conjugation term which determines the basic heat transfer regimes between fluid and solid sections in the microchannel.

By the other hand, Eq. (6) implies the non Newtonian behavior of the fluid in the dimensionless model of the velocity; we take into account the rheological power law model. Zhao (2008) solved the velocity distributions to a slit microchannel whit an analytical solution considering only the electrokinetic forces of electro-osmotic flow of power law fluids for a steady and fully developed flow. This work included the pressure forces in the momentum equation where the velocity profile in physical variables is given by

$$u = -\frac{p_x}{m\kappa^{\left(\frac{n+1}{n}\right)}}\frac{n(\kappa H)^{\left(\frac{n+1}{n}\right)}}{n+1}\left[1-\left(\frac{\kappa y}{\kappa H}\right)^{\frac{n+1}{n}}\right] - \frac{\kappa^{\left(\frac{1-n}{n}\right)}(\in \zeta E_x/m)^{\frac{1}{n}}}{\cosh^{1/n}(\kappa H)}\int_{\kappa y}^{\kappa H}\sinh^{1/n}(\kappa y)\,d(\kappa y); \quad (10)$$

we considering values for the electrokinetic parameter of $\kappa H = \bar{\kappa} \gg 1$, then to solve the integral in the above equation can be used the follow approximation $\sinh(\kappa y) \approx \kappa y$ for $0 \le \kappa y \le 1$ and $\sinh(\kappa y) \approx (1/2)\exp(\kappa y)$ for $\kappa y > 1$. So, the dimensionless model of velocity is given by two sections respectively to the velocity profile

first, to $0 \le \eta \le (1/\bar{\kappa})$,

$$\bar{u}_1 = \frac{u}{u_S} = -\Gamma\left[1-\eta^{\frac{n+1}{n}}\right] + \frac{\left[\frac{1}{n+1}\left\{1-(\bar{\kappa}\eta)^{\frac{n+1}{n}}\right\}\right] + \frac{1}{2^{1/n}}\left[\exp\left(\frac{\bar{\kappa}}{n}\right)-\exp\left(\frac{1}{n}\right)\right]}{\cosh^{1/n}(\bar{\kappa})}, \quad (11a)$$

and second to $(1/\bar{\kappa}) > \eta \le 1$,

$$\bar{u}_2 = \frac{u}{u_S} = -\Gamma\left[1-\eta^{\frac{n+1}{n}}\right] + \frac{\frac{1}{2^{1/n}}\left[\exp\left(\frac{\bar{\kappa}}{n}\right)-\exp\left(\frac{\bar{\kappa}\eta}{n}\right)\right]}{\cosh^{1/n}(\bar{\kappa})}, \quad (11b)$$

where

$$\Gamma = -\frac{\dfrac{p_x}{m\kappa^{(n+1/n)}}\dfrac{n(\kappa H)^{(n+1/n)}}{(n+1)}}{n\kappa^{(1-n/n)}\left(\dfrac{\in \zeta E_x}{m}\right)^{1/n}}, \quad (12)$$

where Γ, is the ratio of pressure forces on electro-osmotic forces.

Now, from the appropriate dimensionless variables from Eq. (5) and (9) in Eq. (3-4) is obtained the dimensionless energy equation to the solid region in the microchannel

$$\bar{\alpha}\frac{\partial \theta_w}{\partial \chi^2} + \frac{\bar{\alpha}}{\bar{\varepsilon}^2}\frac{\partial^2 \theta_w}{\partial Z^2} = 0, \quad (13)$$

and their boundary conditions

$$\chi = 0 : \frac{\partial \theta_w}{\partial \chi} = 0, \quad (14a)$$

$$\chi = 1 : \frac{\partial \theta_w}{\partial \chi} = 0, \tag{14b}$$

$$Z = 0 : \theta = \theta_w, \tag{14c}$$

in addition to Eq. (14c) was considered the boundary condition in the internal interface of microchannel from the Eq. (8). And, to complete the dimensionless energy equation in solid region was considered the next boundary condition in the external interface of microchannel wall

$$\left. \frac{\partial \theta_w}{\partial Z} \right|_{Z=1} = -\frac{\bar{\varepsilon}^2}{\bar{\alpha}} \Lambda, \tag{15}$$

where

$$\Lambda = \frac{q_0''}{\sigma E_x^2 H}, \tag{16}$$

Λ, is the normalized power generation term being the ratio of heat flux from the external wall to the Joule heating.

2.3 Numerical Solution

The previous mathematical model was discretized in central finite differences and solved by the iterative method Successive-Over-Relaxation (SOR), (Hoffman, 2001). In the SOR method, the temperature is evaluated in successive iterations by

$$\theta_{i,j}^{k+1} = \theta_{i,j}^k + \varpi \Delta \theta_{i,j}^{k+1}, \tag{17}$$

where i, j are the nodal positions in axial and transversal direction; k, ϖ and $\Delta \theta_{i,j}^{k+1}$ are the iteration number, the relaxation factor in the SOR method and the dimensionless temperature variation per iteration and node of the discretized mesh, respectively. Eq. (17) is applicable for the solid and fluid regions.

Fluid region: The temperature $\theta_{i,j}^{k+1}$ variation of the interiors nodes that not correspond to boundary nodes was determined by

$$\Delta \theta_{i,j}^{k+1} = \frac{\left[\beta^2 - \frac{\Delta \chi \beta Pe \bar{u}_j}{2} \right] \theta_{i+1,j} + \Omega^2 \theta_{i,j+1} + \left[\beta^2 + \frac{\Delta \chi \beta Pe \bar{u}_j}{2} \right] \theta_{i-1,j} + \Omega^2 \theta_{i,j-1} - 2 \left(\beta^2 + \Omega^2 \right) \theta_{i,j} + \Delta \chi^2}{2 \left(\beta^2 + \Omega^2 \right)}, \tag{18}$$

where $\Omega = \Delta \chi / \Delta \eta$ is the aspect ratio of the discretized mesh for the fluid region; $\Delta \chi$ and $\Delta \eta$ are the increments in the axial and transversal direction respectively. For the dimensionless velocity $\bar{u}_j$ in the Eq. (11), η is replaced by $\eta_j = j \Delta \eta$.

The specified temperature in the inlet of microchannel, as boundary condition is from Eq. (7a) is

$$\theta(i,j) = 0, \text{ for } i = 0, j = 0 \text{ to } jmax, \tag{19}$$

where $jmax$, is the maximum number of nodes in the transversal coordinate.

The boundary conditions in the fluid region which are not specified temperature were adapted to the SOR method as follows; at the outlet of microchannel from de Eq. (7b) gives

$$\Delta\theta_{i,j}^{k+1} = \frac{\Omega^2\theta_{i,j+1} + 2\beta^2\theta_{i-1,j} + \Omega^2\theta_{i,j-1} - 2(\beta^2+\Omega^2)\theta_{i,j} + \Delta\chi^2 + \left[\beta^2 - \dfrac{\Delta\chi\beta Pe\bar{u}_j}{2}\right]2\Delta\chi F_{x2}}{2(\beta^2+\Omega^2)}, \quad (20)$$

where $F_{x2} = (\partial\theta/\partial\chi)\big|_{\chi=1} = 0$; for $i = imax$; $j = 1$ to $jmax\text{-}1$. $imax$, is the maximum number of nodes in the axial coordinate.

The boundary condition at the center of microchannel from the Eq. (7c) gives

$$\Delta\theta_{i,j}^{k+1} = \frac{\left[\beta^2 - \dfrac{\Delta\chi\beta Pe\bar{u}_j}{2}\right]\theta_{i+1,j} + 2\Omega^2\theta_{i,j+1} + \left[\beta^2 + \dfrac{\Delta\chi\beta Pe\bar{u}_j}{2}\right]\theta_{i-1,j} - 2(\beta^2+\Omega^2)\theta_{i,j} + \Delta\chi^2 - 2\Omega^2\Delta\eta F_{y1}}{2(\beta^2+\Omega^2)}, (21)$$

where $F_{y1} = (\partial\theta/\partial\eta)\big|_{\eta=0} = 0$, for $j = 0$; $i = 1$ to $imax\text{-}1$.

The specified temperature in the internal interface of microchannel as boundary condition is from Eq. (7d) is

$$\theta(i,j) = \theta_W(i,j), \text{ for } j = jmax, i = 0 \text{ to } imax. \quad (22)$$

In addition to the internal interface of microchannel requires an equation to solve the boundary nodes, from Eq. (8) is obtained

$$\Delta\theta_{i,j}^{k+1} = \frac{\left[\beta^2 - \dfrac{\Delta\chi\beta Pe\bar{u}_j}{2}\right]\theta_{i+1,j} + 2\Omega^2\theta_{i,j-1} + \left[\beta^2 + \dfrac{\Delta\chi\beta Pe\bar{u}_j}{2}\right]\theta_{i-1,j} - 2(\beta^2+\Omega^2)\theta_{i,j} + \Delta\chi^2 + 2\Omega^2\Delta\eta F_{y2(i,j)}}{2(\beta^2+\Omega^2)}, (23)$$

where $F_{y2(i,j)} = \dfrac{\bar{\alpha}}{\bar{\varepsilon}^2}\dfrac{\partial\theta_{w,i,j}}{\partial Z}\bigg|_{Z=0}$ for $j = jmax, i = 1$ to $imax\text{-}1$.

The boundary conditions for the corner node $i = imax$, $j = 0$, were discretized from the Eqs. (7b, c) considering the outlet and the middle conditions of microchannel in these node, respectively, obtaining

$$\Delta\theta_{i,j}^{k+1} = \frac{2\beta^2\theta_{i-1,j} + 2\Omega^2\theta_{i,j+1} - 2(\beta^2+\Omega^2)\theta_{i,j} + \Delta\chi^2 - 2\Delta\eta\Omega^2 F_{y1} + \left[\beta^2 - \dfrac{\Delta\chi\beta Pe\bar{u}_j}{2}\right]2\Delta\chi F_{x2}}{2(\beta^2+\Omega^2)}, \quad (24)$$

In the same way, the boundary conditions for the corner node $i = imax$, $j = jmax$, were discretized from the Eqs. (7b) and (8) considering the outlet and the internal interface conditions of microchannel in these node, respectively, obtaining

$$\Delta\theta_{i,j}^{k+1} = \frac{2\beta^2\theta_{i-1,j} + 2\Omega^2\theta_{i,j-1} - 2\left(\beta^2 + \Omega^2\right)\theta_{i,j} + \Delta\chi^2 + \left[\beta^2 - \dfrac{\Delta\chi\beta Pe\bar{u}_j}{2}\right]2\Delta\chi F_{x2} + 2\Omega^2\Delta\eta F_{y2(i,j)}}{2\left(\beta^2 + \Omega^2\right)}. \quad (25)$$

Solid region: The temperature $\theta_{w,i,j}^{k+1}$ variation of the interiors nodes that not correspond to boundary nodes was determined by

$$\Delta\theta_{w,i,j}^{k+1} = \frac{\bar{\alpha}\theta_{w,i+1,j} + \dfrac{\bar{\alpha}}{\bar{\varepsilon}^2}\Phi^2\theta_{w,i,j+1} + \bar{\alpha}\theta_{w,i-1,j} + \dfrac{\bar{\alpha}}{\bar{\varepsilon}^2}\Phi^2\theta_{w,i,j-1} - 2\bar{\alpha}\left(1 + \dfrac{\Phi^2}{\bar{\varepsilon}^2}\right)\theta_{w,i,j}}{2\bar{\alpha}\left(1 + \dfrac{\Phi^2}{\bar{\varepsilon}^2}\right)}, \quad (26)$$

where $\Phi = \Delta\chi/\Delta Z$, is the aspect ratio of the discretized mesh for the solid region; ΔZ is the increment in the transverse direction.

The boundary conditions in the solid region which are not specified temperature were adapted to the SOR method as follows; at the left side of the microchannel wall from Eq. (14a) gives

$$\Delta\theta_{w,i,j}^{k+1} = \frac{2\bar{\alpha}\theta_{w,i+1,j} + \dfrac{\bar{\alpha}}{\bar{\varepsilon}^2}\Phi^2\theta_{w,i,j+1} + \dfrac{\bar{\alpha}}{\bar{\varepsilon}^2}\Phi^2\theta_{w,i,j-1} - 2\bar{\alpha}\left(1 + \dfrac{\Phi^2}{\bar{\varepsilon}^2}\right)\theta_{w,i,j} - 2\bar{\alpha}\Delta\chi F_{wx1}}{2\bar{\alpha}\left(1 + \dfrac{\Phi^2}{\bar{\varepsilon}^2}\right)}, \quad (27)$$

where $F_{wx1} = \left(\partial\theta_w/\partial\chi\right)\big|_{\chi=0} = 0$, for $i = 0$; $j = 1$ to *jmax - 1*.

In the same way, the boundary condition at the right side of the microchannel wall from Eq. (14b) gives

$$\Delta\theta_{w,i,j}^{k+1} = \frac{2\bar{\alpha}\theta_{w,i-1,j} + \dfrac{\bar{\alpha}}{\bar{\varepsilon}^2}\Phi^2\theta_{w,i,j+1} + \dfrac{\bar{\alpha}}{\bar{\varepsilon}^2}\Phi^2\theta_{w,i,j-1} - 2\bar{\alpha}\left(1 + \dfrac{\Phi^2}{\bar{\varepsilon}^2}\right)\theta_{w,i,j} + 2\bar{\alpha}\Delta\chi F_{wx2}}{2\bar{\alpha}\left(1 + \dfrac{\Phi^2}{\bar{\varepsilon}^2}\right)}, \quad (28)$$

where $F_{wx2} = \left(\partial\theta_w/\partial\chi\right)\big|_{\chi=1} = 0$, for $i = imax$; $j = 1$ to *jmax - 1*.

The specified temperature in the internal interface of the microchannel wall as boundary condition from Eq. (14c) is

$$\theta_w(i,j) = \theta(i,j), \text{ for } j = 0, i = 0 \text{ to } imax, \quad (29)$$

in addition to Eq. (14c) was considered the condition marked by the Eq. (8) in the internal interface of the microchannel wall, with help from Eq. (29) is evaluated the following

$$\frac{\bar{\alpha}}{\bar{\varepsilon}^2}\frac{\partial\theta_{w,i,j}}{\partial Z}\bigg|_{Z=0} = \frac{\bar{\alpha}}{\bar{\varepsilon}^2}\left(\frac{\theta_{w,i,j+1} - \theta_{w,i,j}}{\Delta Z}\right) = \frac{\partial\theta_{i,j}}{\partial\eta}\bigg|_{\eta=1}, \quad (30)$$

the previous equation is necessary to evaluate $F_{y2(i,j)}$ in the Eqs. (23) and (25) for the fluid region.

Now, the boundary condition at the external interface of the microchannel wall from Eq. (15) gives

$$\Delta\theta_{w,i,j}^{k+1} = \frac{\bar{\alpha}\theta_{w,i+1,j} + 2\frac{\bar{\alpha}}{\bar{\varepsilon}^2}\Phi^2\theta_{w,i,j-1} + \bar{\alpha}\theta_{w,i-1,j} - 2\bar{\alpha}\left(1+\frac{\Phi^2}{\bar{\varepsilon}^2}\right)\theta_{w,i,j} - 2\Lambda\Phi^2\Delta Z}{2\bar{\alpha}\left(1+\frac{\Phi^2}{\bar{\varepsilon}^2}\right)}, \qquad (31)$$

for $j = jmax, i = 1$ to $imax - 1$.

The boundary conditions for the corner node $i = 0$, $j = jmax$ were discretized from the Eqs. (14a) and (15) considering the left side wall condition and the external interface wall condition of microchannel in these node, obtaining

$$\Delta\theta_{w,i,j}^{k+1} = \frac{2\bar{\alpha}\theta_{w,i+1,j} + 2\frac{\bar{\alpha}}{\bar{\varepsilon}^2}\Phi^2\theta_{w,i,j-1} - 2\bar{\alpha}\left(1+\frac{\Phi^2}{\bar{\varepsilon}^2}\right)\theta_{w,i,j} - 2\bar{\alpha}\Delta\chi F_{wx1} - 2\Delta Z\Phi^2\Lambda}{2\bar{\alpha}\left(1+\frac{\Phi^2}{\bar{\varepsilon}^2}\right)}, \qquad (32)$$

in the same way, the boundary conditions for the corner node $i = max$, $j = jmax$ were discretized from the Eqs. (14b) and (15) considering the right side wall condition and the external interface wall condition of microchannel in these node, obtaining

$$\Delta\theta_{w,i,j}^{k+1} = \frac{2\bar{\alpha}\theta_{w,i-1,j} + 2\frac{\bar{\alpha}}{\bar{\varepsilon}^2}\Phi^2\theta_{w,i,j-1} - 2\bar{\alpha}\left(1+\frac{\Phi^2}{\bar{\varepsilon}^2}\right)\theta_{w,i,j} + 2\bar{\alpha}\Delta\chi F_{wx2} - 2\Delta Z\Lambda\Phi^2}{2\bar{\alpha}\left(1+\frac{\Phi^2}{\bar{\varepsilon}^2}\right)}. \qquad (33)$$

Equations (18), (20-21), (23-28) and (31-33) are replaced in an iterative process in Eq. (17) for each node of the discretized mesh that is not specified temperature. The SOR method ends the process when the temperature converges at each node until $\Delta\theta_{i,j}^{k+1} \leq tolerance = tol$. For the conjugate problem, we solved firstly the temperature field in the solid region with an arbitrary specified temperature in the internal interface to initialize the problem, then the temperature gradient in the internal interface of solid wall was calculated by the Eq. (30), and after it was taken to calculate the temperature gradient of fluid region in same Eq. (30); so with this, the temperature field in the fluid region was calculated. Once that the solid and fluid region are solved, we compare the calculated interfacial temperature by $\left|\theta^k(i,j)\right|_{\eta=1} - \theta_w^k(i,j)\Big|_{Z=0}\right| \leq 0.001$, if the previous condition is not satisfied, then the cycle is repeated with the new calculated interfacial temperature in the solid $\theta_w^{k+1}\Big|_{z=0} = \theta^{k+1}\Big|_{\eta=1}$. To implement the discretized mathematical model was used the programming software Fortran Power Station 4.0 and the following parameter values: $\Delta\chi=0.005$, $\Delta\eta=0.005$, $\Delta Z=0.005$, $imax=200$, $jmax=200$, $tol=10^{-8}$.

2.4 Asymptotic Solution

In order to validate the numerical results, we conduct an asymptotic solution for the Eqs. (6) and (13). So, to obtain the relevant dimensionless parameters and the working regimes, we introduce an order of magnitude analysis. Due to the adiabatic boundary conditions at both sides of the microchannel walls, the heat generated by Joule heating is transferred to the fluid. This means that the overall heat transfer from fluid to the microchannel wall have to be of the same order of magnitude

$$\sigma E_x^2 H \sim k_f \frac{\Delta T_f}{H} \sim k_w \frac{\Delta T_w}{H_w} \sim q_0'', \tag{34}$$

where ΔT_w and ΔT_f are the characteristic temperature changes in the transverse direction for the wall and the fluid, respectively. On the other hand, the total temperature change in the system is then of order

$$\Delta T \sim \Delta T_f + \Delta T_w. \tag{35}$$

Combining the Eq. (34) and (35), can be show that

$$\frac{\Delta T_f}{\Delta T} \sim \frac{1}{1 + \dfrac{\bar{\varepsilon}^2}{\bar{\alpha}}}, \tag{36}$$

and

$$\frac{\Delta T_w}{\Delta T} \sim \frac{\dfrac{\bar{\varepsilon}^2}{\bar{\alpha}}}{1 + \dfrac{\bar{\varepsilon}^2}{\bar{\alpha}}}, \tag{37}$$

therefore, the global temperature change must be then of the order

$$\Delta T \sim \frac{\sigma E_x^2 H^2}{k_f} \left[1 + \frac{\bar{\varepsilon}^2}{\bar{\alpha}} \right]. \tag{38}$$

From Eqs. (36) y (37) we can obtain interesting asymptotic relevant limits, which dictate the different physical regimes of the conjugate heat transfer process. Basically, for electro-osmotic flows, typical limits for the dimensionless parameters are $\bar{\alpha}/\bar{\varepsilon}^2 \sim 1$ and $\bar{\alpha}/\bar{\varepsilon}^2 \gg 1$, both with $\bar{\alpha} \ll 1$.

For values of $\bar{\alpha}/\bar{\varepsilon}^2 \sim 1$, from Eq. (36) and (37) we obtain

$$\frac{\Delta T_f}{\Delta T} \sim 1; \frac{\Delta T_w}{\Delta T} \sim 1, \tag{39}$$

thus, the transverse temperature variations in the wall as well as in the fluid (compared with the overall temperature drop, ΔT), are of the same order. For values of $\bar{\alpha}/\bar{\varepsilon}^2 \gg 1$, we obtain from the same order of equations

$$\frac{\Delta T_f}{\Delta T} \sim 1; \frac{\Delta T_w}{\Delta T} \sim \frac{\bar{\varepsilon}^2}{\bar{\alpha}}, \tag{40}$$

so, from Eq. (40), the transverse temperature drop in the fluid is of the same order that the overall temperature drop and the transverse temperature variations in the microchannel wall compared with overall temperature drop ΔT are very small, of order $\bar{\varepsilon}^2/\bar{\alpha} \gg 1$ at most.

The asymptotic solution presented here validates the numerical solution, considering the asymptotic limit $\bar{\alpha}/\bar{\varepsilon}^2 \sim 1$ with $\bar{\alpha} \ll 1$. In this regime, we propose the next regular expansion series, in powers of $\bar{\alpha}$, for the dimensionless temperature in the fluid region

$$\theta = \theta_0(\chi) + \bar{\alpha}\theta_1(\chi,\eta) + ..., \tag{41}$$

and for the solid wall temperature

$$\theta_w = \theta_{w0}(\chi,Z) + \bar{\alpha}\theta_{w1}(\chi,Z) + ..., \tag{42}$$

where we have assumed that the temperature in the fluid is function of χ in a first approximation, and the temperature in the wall depends on χ and Z. So, comparing in orders of magnitude the diffusive terms with the energy generation term in the Eq. (1) for the fluid region, is showed that the significant temperature variations occur in the axial coordinate. Substituting the Eq. (41) into (6)

$$\beta Pe\bar{u}\left[\frac{\partial\theta_0}{\partial\chi} + \bar{\alpha}\frac{\partial\theta_1}{\partial\chi} + ...\right] = \beta^2\left[\frac{\partial^2\theta_0}{\partial\chi^2} + \bar{\alpha}\frac{\partial^2\theta_1}{\partial\chi^2} + ...\right] + \bar{\alpha}\left[\frac{\partial^2\theta_1}{\partial\eta^2} + ...\right] + 1, \tag{43}$$

we can integrate the Eq. (43) in the transversal direction, is obtained

$$\beta Pe\frac{\partial\theta_0}{\partial\chi}\int_{\eta=0}^{\eta=1}\bar{u}d\eta + \bar{\alpha}\beta Pe\frac{\partial\theta_1}{\partial\chi}\int_{\eta=0}^{\eta=1}\bar{u}d\eta =$$
$$\beta^2\frac{\partial^2\theta_0}{\partial\chi^2}\int_{\eta=0}^{\eta=1}d\eta + \bar{\alpha}\beta^2\frac{\partial^2\theta_1}{\partial\chi^2}\int_{\eta=0}^{\eta=1}d\eta + \bar{\alpha}\int_{\eta=0}^{\eta=1}\left(\frac{\partial^2\theta_1}{\partial\eta^2}\right)d\eta + \int_{\eta=0}^{\eta=1}d\eta, \tag{44}$$

but, in considering for cover the integral $\int_{\eta=0}^{\eta=1}\bar{u}d\eta$ from Eq. (11), for the dimensionless velocity, the Eq. (44) for the temperature fields are open at: first region for $0 \leq \eta \leq (1/\bar{\kappa})$ and considering that $(\partial\theta_1/\partial\eta)\big|_{\eta=0} = 0$

$$\beta Pe\frac{\partial\theta_0}{\partial\chi}\int_{\eta=0}^{\eta=1/\bar{\kappa}}\bar{u}_1 d\eta + \bar{\alpha}\beta Pe\frac{\partial\theta_1}{\partial\chi}\int_{\eta=0}^{\eta=1/\bar{\kappa}}\bar{u}_1 d\eta = \frac{\beta^2}{\bar{\kappa}}\frac{\partial^2\theta_0}{\partial\chi^2} + \bar{\alpha}\frac{\beta^2}{\bar{\kappa}}\frac{\partial^2\theta_1}{\partial\chi^2} + \bar{\alpha}\frac{\partial\theta_1}{\partial\eta}\bigg|_{\eta=1/\bar{\kappa}} + \frac{1}{\bar{\kappa}}, \tag{45}$$

after, for the region $(1/\bar{\kappa}) > \eta \leq 1$

$$\beta Pe\frac{\partial\theta_0}{\partial\chi}\int_{\eta=1/\bar{\kappa}}^{\eta=1}\bar{u}_2 d\eta + \bar{\alpha}\beta Pe\frac{\partial\theta_1}{\partial\chi}\int_{\eta=1/\bar{\kappa}}^{\eta=1}\bar{u}_2 d\eta =$$
$$\beta^2\frac{\partial^2\theta_0}{\partial\chi^2}\left(1 - \frac{1}{\bar{\kappa}}\right) + \bar{\alpha}\beta^2\frac{\partial^2\theta_1}{\partial\chi^2}\left(1 - \frac{1}{\bar{\kappa}}\right) + \bar{\alpha}\left(\frac{\partial\theta_1}{\partial\eta}\bigg|_{\eta=1} - \frac{\partial\theta_1}{\partial\eta}\bigg|_{\eta=1/\bar{\kappa}}\right) + \left(1 - \frac{1}{\bar{\kappa}}\right), \tag{46}$$

Where respectively for the each velocity profile

$$\int_{\eta=0}^{\eta=1/\bar{\kappa}} \bar{u}_1 d\eta = \Gamma\left[\frac{n}{2n+1}\left(\frac{1}{\bar{\kappa}}\right)^{\frac{2n+1}{n}} - \frac{1}{\bar{\kappa}}\right] + \frac{1}{(n+1)\cosh^{1/n}(\bar{\kappa})}\left[\frac{1}{\bar{\kappa}} - \frac{n\bar{\kappa}^{(n+1/n)}}{2n+1}\left(\frac{1}{\bar{\kappa}}\right)^{\frac{2n+1}{n}}\right] +$$

$$\frac{\left[\exp\left(\frac{\bar{\kappa}}{n}\right) - \exp\left(\frac{1}{n}\right)\right]}{2^{1/n}\bar{\kappa}\cosh^{1/n}(\bar{\kappa})}, \tag{47a}$$

and

$$\int_{\eta=1/\bar{\kappa}}^{\eta=1} \bar{u}_2 d\eta = -\Gamma\left(1 - \frac{1}{\bar{\kappa}}\right) + \frac{n\Gamma}{2n+1}\left[1 - \left(\frac{1}{\bar{\kappa}}\right)^{\frac{2n+1}{n}}\right] +$$

$$\frac{1}{2^{1/n}\cosh^{1/n}(\bar{\kappa})}\left[\left(1 - \frac{1}{\bar{\kappa}}\right)\exp\left(\frac{\bar{\kappa}}{n}\right) - \frac{n}{\bar{\kappa}}\left\{\exp\left(\frac{\bar{\kappa}}{n}\right) - \exp\left(\frac{1}{n}\right)\right\}\right]. \tag{47b}$$

Now, substituting the expansions from the Eqs. (41) and (42) into the boundary condition given by Eq. (8) and considering that the zero power of θ only depend of $\theta(\chi)$, then $(\partial\theta_0/\partial\eta)|_{\eta=1} = 0$, and simplifying

$$\frac{1}{\bar{\varepsilon}^2}\left[\frac{\partial\theta_{w0}}{\partial Z}\bigg|_{Z=0} + \bar{\alpha}\frac{\partial\theta_{w1}}{\partial Z}\bigg|_{Z=0}\right] = \frac{\partial\theta_1}{\partial\eta}\bigg|_{\eta=1}, \tag{48}$$

for collecting the zero power of $\bar{\alpha}$ from Eq. (48), we get

$$O(\alpha^0): \frac{1}{\bar{\varepsilon}^2}\frac{\partial\theta_{w0}}{\partial Z}\bigg|_{Z=0} = \frac{\partial\theta_1}{\partial\eta}\bigg|_{\eta=1}, \tag{49}$$

also, by considering the limit in $\bar{\alpha} \ll 1$ and $\bar{\alpha}/\bar{\varepsilon}^2 \sim O(1)$ the temperature gradients in the microchannel wall from the Eq. (13) are a constant and then $(\partial\theta_w/\partial Z)|_{Z=1} = (\partial\theta_{w0}/\partial Z)|_{Z=0}$, in these conditions, substituting the Eq. (15) into (49) is obtained

$$\frac{\partial\theta_1}{\partial\eta}\bigg|_{\eta=1} = -\frac{\Lambda}{\bar{\alpha}}. \tag{50}$$

For values characteristics in microchannel applications, we can considering for this work $\bar{\kappa} \gg 1$, so the Eq. (45) has influence in a very short region of the order of $0 \le \eta \le (1/\bar{\kappa})$; then, the distributions temperature fields are given mainly in a first approximation for the region $(1/\bar{\kappa}) > \eta \le 1$ given for Eq. (46). By substituting the Eq. (50) into (46) and collecting the zero power of $\bar{\alpha}$, we get

$$O(\alpha^0): \beta Pe\frac{\partial\theta_0}{\partial\chi}\int_{\eta=1/\bar{\kappa}}^{\eta=1} \bar{u}_2 d\eta = \beta^2\frac{\partial^2\theta_0}{\partial\chi^2} - \Lambda + 1, \tag{51}$$

where $1/\bar{\kappa} \ll 1$, with their corresponding boundary conditions

$$\chi = 0: \theta_0 = 0, \tag{52a}$$

$$\chi = 1 : \frac{\partial \theta_0}{\partial \chi} = 0. \tag{52b}$$

The solution in a first approximation to Eq. (51) is

$$\theta_0(\chi) = \frac{(\Lambda - 1)}{\left(Pe\int_{\eta=1/\bar{\kappa}}^{\eta=1}\bar{u}_2 d\eta\right)^2}\left[\exp\left(\frac{Pe\int_{\eta=1/\bar{\kappa}}^{\eta=1}\bar{u}_2 d\eta}{\beta}(\chi-1)\right) - \exp\left(-\frac{Pe\int_{\eta=1/\bar{\kappa}}^{\eta=1}\bar{u}_2 d\eta}{\beta}\right)\right] + \frac{(1-\Lambda)\chi}{\beta Pe\int_{\eta=1/\bar{\kappa}}^{\eta=1}\bar{u}_2 d\eta},$$
$$\tag{53}$$

Now, by substituting Eq. (42) into (13) and considering the case of the solid region was considered the limit $\bar{\alpha} \ll 1$, and $\bar{\alpha}/\bar{\varepsilon}^2 \sim O(1)$, and by collecting the zero power of $\bar{\alpha}$

$$\frac{\partial^2 \theta_{w0}}{\partial Z^2} = 0, \tag{54}$$

with their corresponding boundary conditions

$$Z = 0 : \theta_0 = \theta_{w0}, \tag{55}$$

and the condition market with Eq. (15). Therefore the analytical solution in a first approximation to the energy equation to the solid region is

$$\theta_{w0}(\chi, Z) = -\frac{\bar{\varepsilon}^2}{\bar{\alpha}}\Lambda Z + \theta_0(\chi) \tag{56}$$

3　RESULTS AND DISCUSSIONS

In this study, we consider the order of magnitude of the following characteristic values: $H \sim 10^{-4}m$, $H_W \sim 10^{-5}m$, $L \sim 10^{-2}m$; $\bar{\kappa} \sim 100$, based in a 0.001 mM buffer solution and symmetrical electrolyte; thermal properties of materials were taken as $k_f = 0.61 - 0.7 W/m \cdot K$, $k_w = 0.15 - 0.19 W/m \cdot K$, $k_w = 1.38 W/m \cdot K$ for the fluid, PMMA polymer wall and fused silica wall, respectively; $\sigma \sim 10^{-3} - 10^{-2} S/m$; $u_{HS} \sim 10^{-4} - 10^{-3}m/s$, $\epsilon \sim 10^{-10}C/m \cdot V$, $\zeta \le 10^{-2}V$, $E_x \sim 10^4 - 10^5 V/m$ and $\eta_0 \sim 10^{-3} - 10^{-4}Pa \cdot s$, $\rho \sim 10^3 kg/m^3$, $C_p = 4180 J/kg \cdot K$. Therefore $\beta \sim 0.01$ and $\bar{\varepsilon} \sim 0.001$; $\bar{\alpha} \sim 2.5x10^{-6} - 2.5x10^{-5}$; $Pe \sim 0.1 - 1.0$. $-1 \le \Gamma \le 1$, $n \sim 0.5 - 1.5$ (Afonso, 2009); $\Lambda = 1, 0.75, 0.5$ (Das and Chakraborty, 2006).

Figure 2 show the dimensionless velocity distributions for different values of the fluid behavior index, $n(= 0.5, 0.8, 1, 1.2, 1.5)$, while keeping $\bar{\kappa} = 100$; is neglect the pressure effect $\Gamma = 0$. The dimensionless velocity was obtained using the generalized Soluchowski velocity u_S for power law fluids. It be can see that the irrespective of value of the fluid behavior index, the velocity near of the center of the microchannel approaches to the generalized Soluchowski velocity; so, the velocity profiles becomes more plug-like as the fluid behavior index decrease. To $n = 1$, the Newtonian case is recovered.

In the case that; it will be recovered de Newtonian case with $n=1$, the Figure 3 show the influence of the ratio of pressure forces on electro-osmotic forces for different values to $\Gamma(=-1,0,1)$. For negative and positive values of Γ, its acts as a drag increaser and drag reducer on the flow, respectively. For $\Gamma=0$ the velocity profiles correspond to a plug-like flow, due to the solely action of electro-osmotic forces.
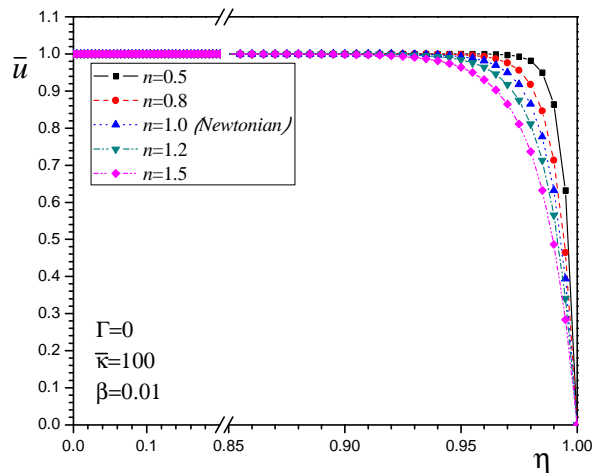
Figure 2. Dimensionless velocity distributions for different values of the fluid behavior index, *n*, while keeping $\bar{\kappa}=100$ and $\Gamma=0$.
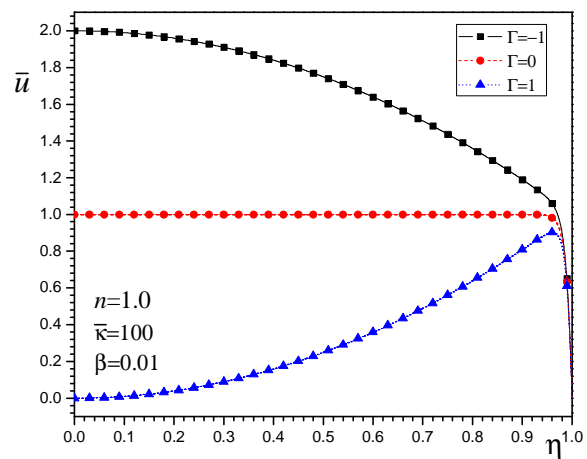
Figure 3. Dimensionless velocity distributions for different values of the ratio of pressure forces on electro-osmotic forces, Γ, while keeping $\bar{\kappa}=100$ and $n=1$.

The mixed effect of the pressure and electro-osmotic forces in the velocity profiles of flow is showed in the Figure 4 when $\Gamma=-1$ acts as drag increaser, for different values of $n(=0.5,1,1.5)$ and a fixed value of $\bar{\kappa}=100$. We can see, that for values of $n<1$ (pseudoplastic liquids) the velocity profile tends to increase in the flow direction upper Newtonian case $(n=1)$, while the electro-osmotic effect is clearly marked having the larger values of velocity near of the microchannel wall, because this kind of fluids has smaller wall dynamic viscosity (Zhao, 2008). For values of $n>1$ (dilatants liquids) the velocity profile tends to decrease in the flow direction below Newtonian case, while the electro-osmotic effect is less in the wall, having the smaller values of velocity near of the microchannel wall, because this kind of fluids has higher wall dynamic viscosity, having a less influence of the external electric field (Zhao, 2008).

The Figure 5 show the mixed effect of the pressure and electro-osmotic forces in the velocity profiles of flow when $\Gamma=1$ acts as drag decreaser, for different values of $n(=0.5,1,1.5)$ and a fixed value of $\bar{\kappa}=100$. The effect of *n* over the velocity profiles near of the microchannel wall is very similar to mentioned in Figure 4. But, the viscosity effect over the velocity profiles toward the center of microchannel in a pseudoplastic liquids ($n<1$) with an adverse pressure gradient makes the velocity profiles are below that Newtonian case (contrary to established with a favorable pressure gradient in Figure 4). While for dilatants liquids $(n>1)$ with an adverse pressure gradient makes the velocity profiles are upper that Newtonian case (contrary to established with a favorable pressure gradient in Figure 4).
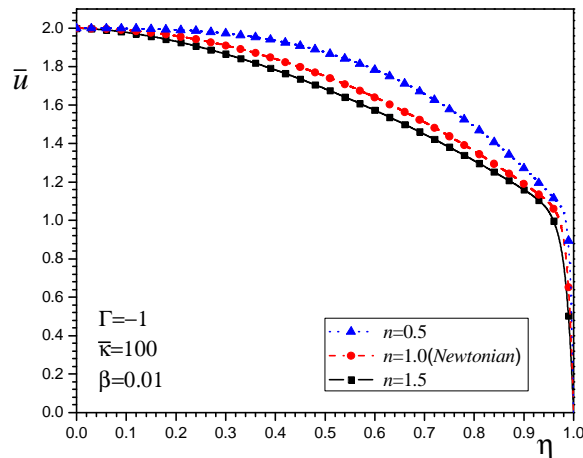
Figure 4. Dimensionless velocity distributions for different values of the fluid behavior index, n, while keeping $\bar{\kappa}=100$ and $\Gamma=-1$.
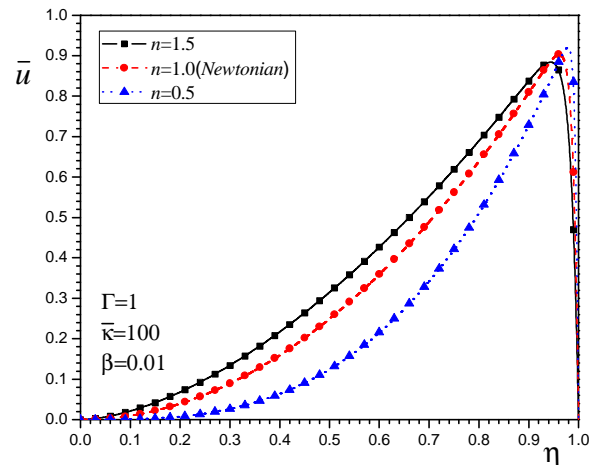
Figure 5. Dimensionless velocity distributions for different values of the fluid behavior index, n, while keeping $\bar{\kappa}=100$ and $\Gamma=1$.

Figure 6 and 7, shows the dimensionless velocity distributions for different values of the electrokinetic parameter $\bar{\kappa}(=10,50,100)$, while keeping $\Gamma=0$. Then is neglect the pressure effect. It can be see that for an irrespective value of the fluid behavior index, the velocity near of the center of the microchannel approaches to the generalized Soluchowski velocity. The velocity profile becomes more plug-like as the fluid behavior index decrease $(n<1)$, as shown by the Figure 6. While for values for $(n>1)$ the effect by the electric field near of the wall of microchannel is less, away the plug-like pattern in the velocity profiles, as shown by the Figure 7. The influence of the electrokinetic parameter $\bar{\kappa}$ is clear in the Figures 6-7, for small values of $\bar{\kappa}(<10)$ indicates a big size of the EDL respect the size of microchannel (tending to overlap of EDLs) and therefore a low influence for the external electric field near of the microchannel wall, leaving a parabolic pattern in the velocity profiles. By other hand, for values of $\bar{\kappa}(\gg 10)$ indicates a small size of the EDL respect to the size of microchannel and therefore a high influence for the external electric field near of the microchannel wall; leaving a plug –like pattern in the velocity profiles.

The Figure 8 shows the spatial development of the Joule heating induced to the fluid and the wall temperature profiles in the microchannel, along the transversal direction in the middle axial position for different values of $n(=0.5,1,1.5)$ and $\Gamma=0$. The temperature distributions in the fluid region exhibit a parabolic-like pattern while the solid wall exhibits a linear behavior (Tang, 2004b). It also shows that the highest temperature occurs at the microchannel centerline; for that is clear that the heat generated by Joule heating is transferred from the central region to wall by convection and conduction in the fluid, and dissipated through the microchannel wall by conduction, finally the heat is transferred to the exterior by the q_0''. For the parameters shown in the Figure 8 we can see that for values of the fluid behavior index, $n>1$, with $\Gamma=0$ the velocity profiles decrease causing an increment of the temperature profiles (respect to Newtonian case) reducing the convective effect. And, for $n<1$, with $\Gamma=0$ the velocity profiles increase causing a decrement of the temperature profiles (respect to Newtonian case) increasing the convective effect.

For the parameters shown in the Figure 9, we show the spatial development of the fluid and de wall temperature profiles en the microchannel, along the transversal direction in the middle axial position for different values of $\Gamma(=-1,0,1)$ and $n=0.5$. The influence of the ratio of pressure forces on electro-osmotic forces, Γ, is relevant, because for negative values of $\Gamma(=-1)$ acts a drag increaser on the flow, decreasing the temperature profiles of system by increasing the convective effects. On the other hand, for positive values of $\Gamma(=1)$, its acts a drag reducer on the flow therefore causing an increase of temperature profiles by decreasing the convective effects. Then $\Gamma<0$ and $\Gamma>0$ correspond to Poiseuille electro-osmotic flows with favorable and adverse pressure gradients, respectively. For $\Gamma=0$ the velocity profiles correspond to a plug-like flow, due to the solely action of electro-osmotic forces and their temperature profiles are showed in Figure 9.
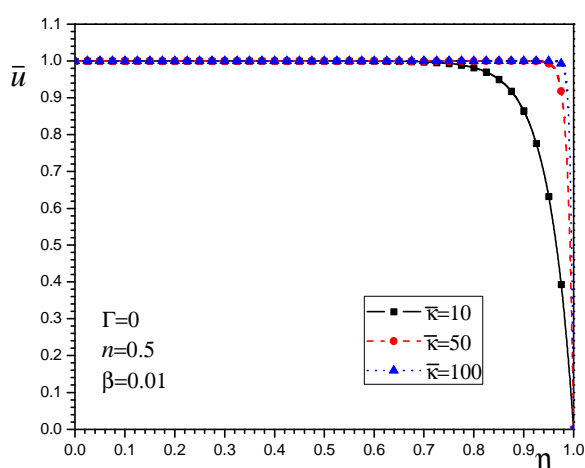
Figure 6. Dimensionless velocity distributions for different values of the electrokinetic parameter, $\bar{\kappa}$, while keeping $\Gamma=0$ and $n=0.5$.
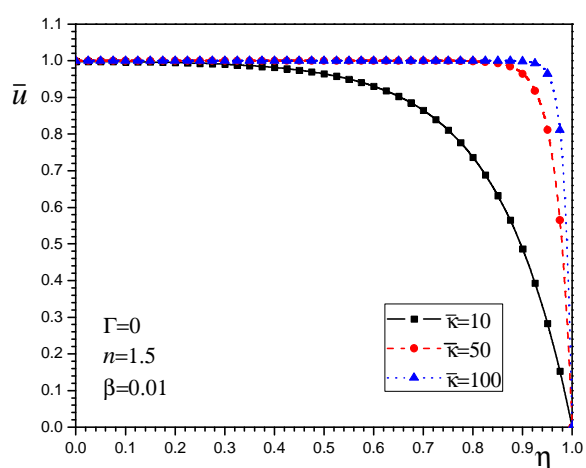
Figure 7. Dimensionless velocity distributions for different values of the electrokinetic parameter, $\bar{\kappa}$, while keeping $\Gamma=0$ and $n=1.5$.
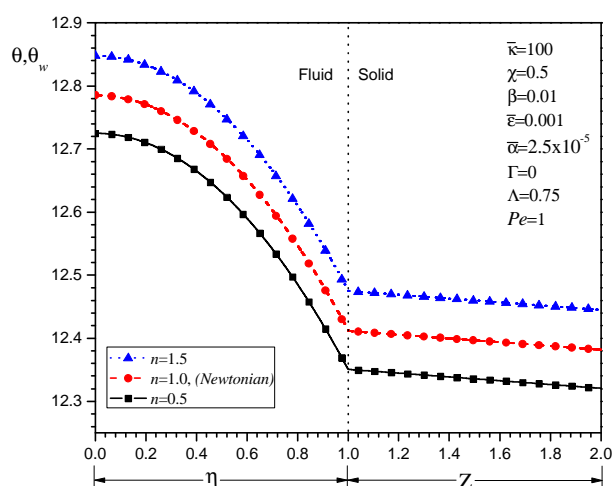
Figure 8. Dimensionless temperature profile as a function of dimensionless transversal coordinate in the fluid and solid region, at $\chi=0.5$ for different values of the flow consistency index, n, while keeping $\Gamma=0$.
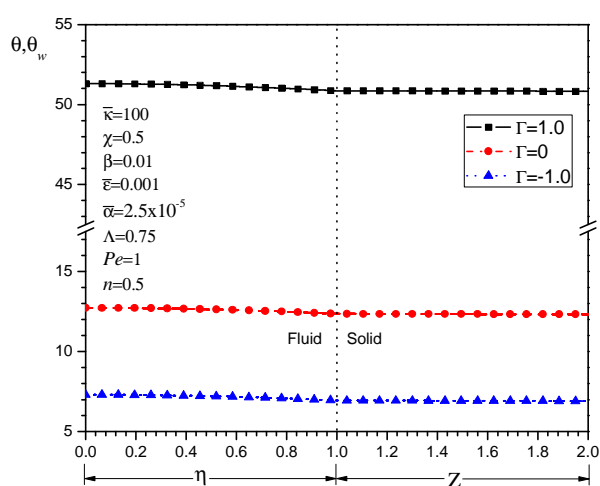
Figure 9. Dimensionless temperature profile as a function of dimensionless transversal coordinate in the fluid and solid region, at $\chi=0.5$ for different values of the ratio of pressure forces on electro-osmotic forces, Γ, while keeping $n=0.5$.

For the parameters shown in the Figure 10, show the spatial development of the fluid and de wall temperature fields en the microchannel along transversal direction for different values of $\chi(=0.1, 0.5, 1)$, $n = 0.5$, and $\Gamma = 0$. We can see a constant increase of Joule heating toward the outlet of the microchannel, practically a linear increment of the temperature in the longitudinal coordinate.

The Figure 11 shows that for decrease of *Pe* number the convection effect decrease also, over the conduction effect, increasing the temperature profiles significantly. So the *Pe* number is an indicator of the convection velocity in the system.
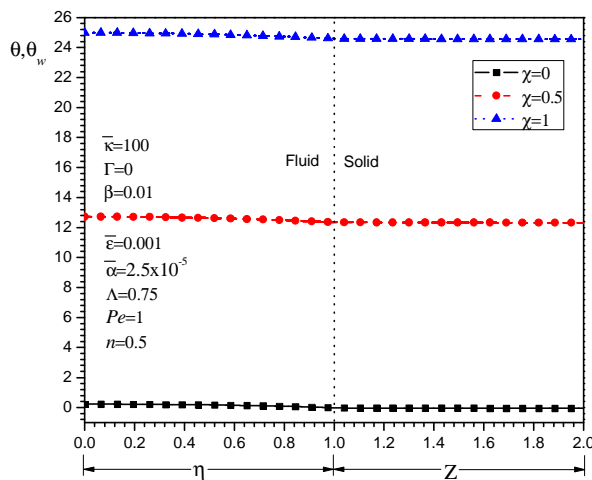
Figure 10. Dimensionless temperature profile as a function of dimensionless transversal coordinate in the fluid and solid region, for different values of the axial coordinate, χ, while keeping $\Gamma = 0$ and $n = 0.5$.
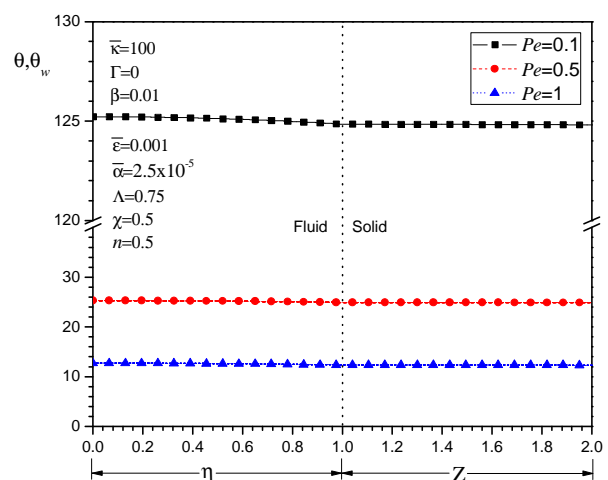
Figure 11. Dimensionless temperature profile as a function of dimensionless transversal coordinate in the fluid and solid region, for different values of the Peclet number, *Pe*, while keeping $\Gamma = 0$ and $n = 0.5$.

The Figure 12 depicts the temperature profiles across transversal direction of microchannel in the middle axial length for the fluid and solid region, for $\Lambda(=1, 0.75, 0.5)$, $n = 0.5$, and $\Gamma = 0$. In all cases the value of q_0'' is considered as a constant extraction of heat from the channel walls. Is important recall here that the temperature rises in electro-osmotic flows under constant wall heat flux boundary conditions, this may attributed to the combined mechanism of Joule heating and heat transfer in the walls. For the cases studied in the Figure 12, the Joule heating seems to be a dominant mechanism behind temperature increments within the system. In general, for increase the value of Joule heating, the transversal temperature tends to increase. So, from the different temperature profiles we can see that the lower value of Λ, higher is the temperature rise at a given axial location of the microchannel, (Das and Chakraborty, 2006).

The Figure 13 exhibit the influence of the thermal properties in the heat transfer phenomena because by comparing the material of fused silica solid wall with $\bar{\alpha} \sim 2.5 x 10^{-5}$ versus PMMA polymer wall with $\bar{\alpha} \sim 2.5 x 10^{-6}$, we can find the thermal conductivity of PMMA is much lower than that of silica glass. This mean the heat dissipation trough the PMMA wall is more difficult than through the glass wall, leaving an important temperature

changes in solid region, (Tang, 2004b). Then for decrease the value of $\bar{\alpha}$ the temperature gradient in the solid region tend to increase, consequently reducing of the conduction effect.

For the parameters shown, in order to validate the numerical solution from the Eqs. (6-8) the Figure 14 compares the behavior of the axial temperature profile in the fluid region with the asymptotic solution given by Eq. (53); we can see that, in the first approximation for the asymptotic solution is near to the predictions of the axial temperature profile for the fluid region in the numerical solution for three different values of $\Gamma(=-1,0,1)$ and a value of $n(=0.5)$, along the microchannel. In the same way, the Figure 15 shows a zoom with a comparison of numerical an asymptotic solution for the axial temperature profiles for the fluid region for three different values of the flow consistency index $n(=0.5,1,1.5)$ and a value of $\Gamma(=-1)$. The Figure 16 compares the behavior of the transversal temperature profile in the solid region given from the Eq. (8, 13-15) with the asymptotic solution given by Eq. (56); we can see the first approximation for the asymptotic solution of the temperature profile for the solid region with the numerical solution in the middle axial position in the microchannel wall.
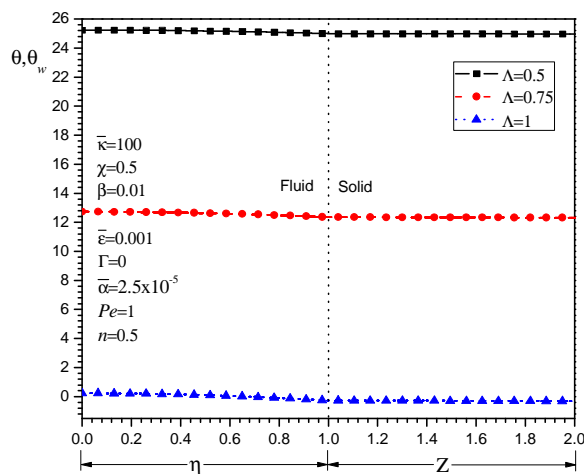
Figure 12. Dimensionless temperature profile as a function of dimensionless transversal coordinate in the fluid and solid region, for different values of the normalized power generation term, Λ, while keeping $\Gamma = 0$ and $n = 0.5$.

Figure 13. Dimensionless temperature profile as a function of dimensionless transversal coordinate in the fluid and solid region, for different values of the conjugation term, $\bar{\alpha}$, while keeping $\Gamma = 0$ and $n = 0.5$.

4 CONCLUSIONS

The present work analyzed different transport characteristics of mixed electro-osmotic and pressure driven flows of non Newtonian fluids, at the same time helps to understand the consequences of the interaction between the applied electric field within the EDL and the result of temperature increase by Joule heating, which has important effects of practical significance. Such Joule heating effects can be significant consequences in low column separation efficiency, reduction of analysis resolution, or even loss of injected samples in biomedical applications. So, the present model can act as a tool towards understanding of the different interconnected transport mechanisms in the efficient design of microfluidic systems.
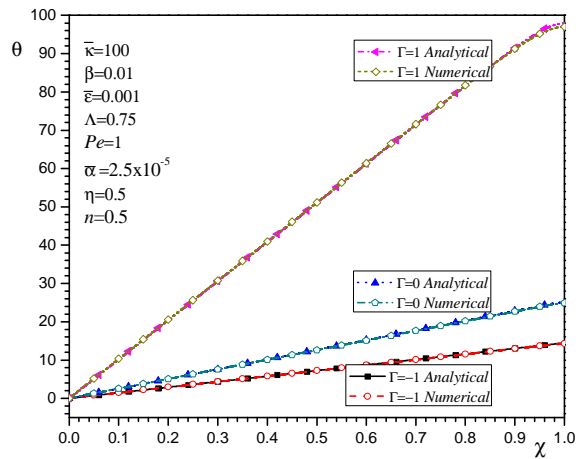
Figure 14. Comparison of the numerical and analytical solution for the spatial development of the temperature profiles in the fluid, along axial direction, for different values of the ratio of pressure forces on electro-osmotic forces, Γ, while keeping $\Lambda = 0.75$ and $n = 0.5$.
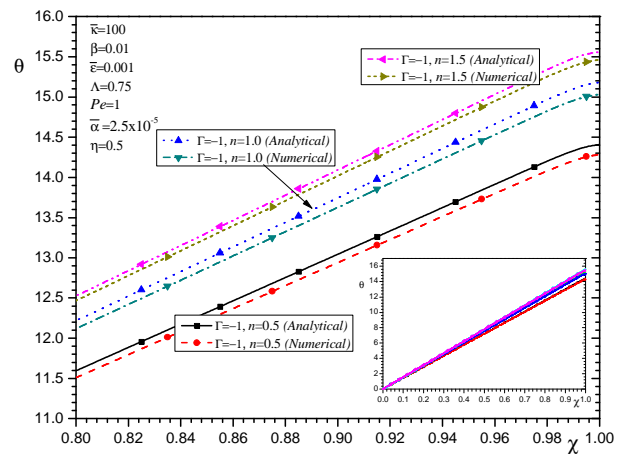
Figure 15. Comparison of the numerical and analytical solution for the spatial development of the temperature profiles in the fluid, along axial direction, for different values of the flow consistency index, n, while keeping $\Gamma = -1$ and $\Lambda = 0.75$.
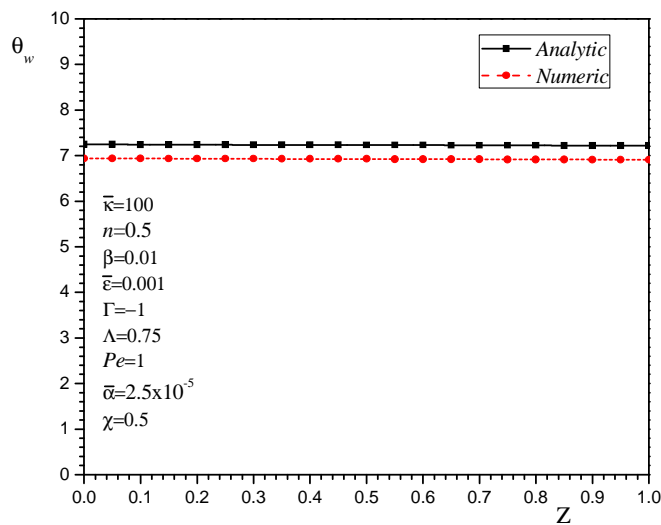
Figure 16. Comparison of the numerical and analytical solution for the spatial development of the temperature profiles in the solid, along transversal direction.

5   ACKNOWLEDGMENTS

6   NOMENCLATURE

C_p Specific heat [J/kg K]

E_x Electric field along the axis of the microchannel [V/m]

F_{wx1}	Temperature gradient in the left side of microchannel wall
F_{wx2}	Temperature gradient in the right side of microchannel wall
F_{x2}	Temperature gradient in the outlet of microchannel
F_{y1}	Temperature gradient in the center of microchannel
$F_{y2(i,j)}$	Temperature gradient in the internal interface of microchannel
H	Half of microchannel [m]
H_w	Wall thickness of the microchannel [m]
$imax$	Maximum numbers of nodes in the axial coordinate
$jmax$	Maximum numbers of nodes in the transversal coordinate
k	Thermal conductivity [W/m-K]
L	Length of microchannel [m]
m	Flow behavior index [Pa·s^n]
n	Flow consistency index
p_x	Pressure gradient in axial direction [N/m^2]
Pe	Peclet number
q_0''	Heat flux at the wall in the region $0 \le x \le L$ [W/m^2]
T	Temperature [K]
T_e	Microchannel inlet temperature [K]
u	Fluid axial velocity [m/s]
$\bar{u}$	Dimensionless fluid axial velocity
u_S	Generalized Soluchowski velocity for power law fluids [m/s]
w	Depth of the microchannel [m]
x	Axial coordinate [m]
y	Transversal coordinate [m]

Greek symbols

$\bar{\alpha}$	Conjugation term
β	Aspect ratio of the fluid region
Γ	Ratio of pressure forces on electro-osmotic forces
$\Delta\eta$	Increment in the transversal direction of fluid
$\Delta\theta$	Dimensionless temperature variation in the fluid region
$\Delta\theta_w$	Dimensionless temperature variation in the solid region
$\Delta\chi$	Increment in the axial direction of fluid and solid
ΔZ	Increment in the transversal direction of solid
$\bar{\varepsilon}$	Aspect ratio of the solid region
Z	Dimensionless transversal coordinate of the solid wall
ζ	Zeta potential in the shear plane of the EDL [V]
η	Dimensionless transversal coordinate of the fluid region
θ	Dimensionless fluid temperature
θ_w	Dimensionless solid temperature
κ	Inverse Debye length [m^{-1}]
$\bar{\kappa}$	Electrokinetic parameter
Λ	Ratio of heat flux from the external wall to the Joule heating
ρ	Fluid density [kg/m^3]
σ	Electrical conductivity of the fluid [S/m]
Φ	Aspect ratio of the mesh in the solid
χ	Dimensionless axial coordinate
Ω	Aspect ratio of the mesh in the fluid

ϖ Relaxation factor of SOR method
Other symbols
ϵ Dielectric constant [C/V-m]
Subscripts
f Fluid
i Nodal position in the axial direction
j Nodal position in the transversal direction
w Wall
superscripts
k Iteration

REFERENCES

Afonso A.M., Alves M.A., Pinho F.T., Analytical solution of mixed electro-osmotic/pressure driven flows of viscoelastic fluids in microchannels, *Journal of Non-Newtonian Fluid Mechanics*, 50–63, 2009.

Berli C.L.A., Olivares M.L., Electrokinetic flow of non-Newtonian fluids in microchannels, *Journal of Colloid and Interface Science*, 320: 582–589, 2008.

Das S., Chakraborty S., Analytical solutions for velocity, temperature and concentration distribution in electroosmotic microchannel flows of a non-Newtonian bio-fluid, *Analytica Chimica Acta*, 559: 15–24, 2006.

Hoffman J.D., *Numerical Methods for Engineers and Scientist*. Marcel Dekker, Inc., Chap. 5, 9, 2001.

Karniadakis G., Beskok A., Aluru N., *Microflows and Nanoflows. Interdiciplinary Applied Mathematics*. Springer, V. 29, Chap. 7, 2005.

Li D., *Electrokinetics in Microfluidics*. Interface Science and Technology, Elsevier Academy Press, V. 2, 2004.

Masliyah J. H., Bhattacharjee S., *Electrokinetic and Colloid Transport Phenomena*. Wiley Interscience, 2006.

Park H.M. and Lee W.M., Helmholtz – Smulochowski velocity for viscoelastic electroosmotic flows, *Journal of Colloid and Interface Science*, 317: 631–636, 2008.

Tang G., Yan D., Gong H., Chai C. and Lam Y., Joule heating and its effects on electrokinetic transport of solutes in rectangular microchannels. *Sensors and Actuators A,* 139:221-232, 2007.

Tang G.H., Li X.F., He Y.L., Tao W. Q, Electroosmotic flow of non-Newtonian fluid in microchannels, *Journal of Non-Newtonian Fluid Mechanics*, 157: 133–137, 2009.

Tang G.Y., Yang C., Chai C.K., and Gong H.Q., Numerical analysis of the thermal effect on electroosmotic flow and electrokinetic mass transport in microchannels, *Analytica Chemica Acta*, 507: 27–37, 2004b.

Tang G.Y., Yang C., Chai J.C., Gong H.Q., Joule heating effect on electroosmotic flow and mass species transport in microcapillary. *International Journal of Heat and Mass Transfer*, 47:215–227, 2004a.

Xuan X., Sinton D., Li D., Thermal end effects on electroosmotic flow in a capillary, *International Journal of Heat and Mass Transfer*, 47:3145–3157, 2004a.

Xuan X., Xu B., Sinton D. and Li D., Electroosmotic flow with Joule heating effects. *Miniaturisation for Chemistry, Biology & Bioengineering Lab Chip*, 4:230–236, 2004b.

Zhao C., Zholkovskij E., Masliyah J. H., and Yang C., Analysis of electroosmotic flow of power-law fluids in a slit microchannel. *Journal of Colloid and Interface Science*, 326:503-510, 2008.